Available online at www.sciencedirect.com
ScienceDirect
Applied Catalysis B: Environmental 78 (2008) 315–323
APPLIED CATALYSIS B: ENVIRONMENTAL
www.elsevier.com/locate/apcatb

Impact of copper on the performance and sulfur tolerance of barium-based NO_x storage-reduction catalysts

Sonia Hammache [a], Lindsey R. Evans [b], Eric N. Coker [b], James E. Miller [b,*]

[a] University of New Mexico, Department of Chemistry and Advanced Materials Laboratories, 1001 University Blvd SE, Albuquerque, NM 87106, USA
[b] Sandia National Laboratories, Advanced Materials Laboratories, 1001 University Blvd SE, Albuquerque, NM 87106, USA

Received 25 July 2006; received in revised form 10 September 2007; accepted 13 September 2007
Available online 18 September 2007

Abstract

The presence of sulfur in automotive exhaust is known to be detrimental to lean-NO_x traps as SO_2 is oxidized to SO_3 that competes with NO_2 for sites on the trap and is difficult to remove. In this study the effect of adding Cu to the prototypical Pt–BaO/γ-Al_2O_3 formulation on the system's tolerance for sulfur was investigated. It was found that in the absence of sulfur, Cu decreases the performance in terms of both NO_x storage capacity and reduction of NO_x to N_2 during regeneration. In the presence of SO_2, Cu provides a significant improvement in sulfur tolerance so that, after sulfur exposure, the storage capacity of the Cu-modified material can exceed that of the baseline material. The sulfur tolerance afforded by Cu is attributed to a moderation in the activity for SO_2 oxidation resulting from the formation of a Pt–Cu bimetallic phase. The propensity for NO oxidation is also modified, but to a lesser effect. Evidence for the bimetallic phase is provided by temperature-programmed reduction (TPR) and electron microscopy. The impact of SO_2 on the Cu-modified material is greater during the regenerative reduction cycle. In this case, the results suggest that sulfur blocks Pt and possibly Cu sites and that the sulfur is not removed by oxidation during the subsequent storage cycle. Hence, activity lost during the reduction cycle is not restored. In contrast, sulfur that blocks Pt sites on the baseline material during the reduction cycle is subsequently oxidized and desorbs from the Pt, restoring the activity. However, some of the resulting SO_3 reacts with the BaO to form $BaSO_4$, and there is a partial loss of storage capacity.
Published by Elsevier B.V.

Keywords: Lean-NO_x trap; NO_x storage reduction; Deactivation; Pt–BaO/γ-Al_2O_3; Pt–Cu–BaO/γ-Al_2O_3

1. Introduction

Fuel economy can be improved and CO_2 emissions decreased by replacing stoichiometric gasoline automotive engines with lean-burn gasoline and diesel designs. However, the current technology for NO_x reduction, the three-way catalyst, is not applicable to an oxygen-rich environment. A catalyst that is effective under lean conditions is therefore needed before the full benefits of lean-burn engines can be realized. Two processes have been developed for this purpose. The first, selective catalytic reduction, is already widely used for stationary NO_x sources, but would require on-board storage and periodic replenishing of the reducing agent, urea or ammonia, or the sacrifice of a portion of the fuel if hydrocarbons are used as reducing agent. The second process which is potentially more transparent to the consumer, NO_x storage-reduction (NSR) catalysts, commonly referred to as lean-NO_x traps, was first proposed by Toyota [1,2] and is based on the principle of alternating between long fuel-lean cycles during which NO_x is captured and stored, and short fuel-rich cycles wherein the trap is regenerated and NO_x is reduced to N_2. NSR catalysts generally contain a noble metal component and an alkaline oxide. The most common and well-characterized formulation is Pt–BaO/γ-Al_2O_3 [1]. It is generally accepted that during the lean storage cycle the noble metal oxidizes NO to NO_2, and then the NO_2 is stored as an alkali nitrate. During the reduction or regeneration cycle, the nitrates are decomposed and reduced by the hydrocarbons to N_2.

One shortcoming of the NSR approach is the catalysts are quite susceptible to sulfur poisoning. That is, the alkaline oxides, being good traps for NO_x, are good traps for SO_x as well. The adsorption of SO_2 on the NSR catalyst occurs in a similar manner as the adsorption of NO_x, i.e. the oxidation of SO_2 to SO_3 followed by the adsorption of SO_3 on the alkaline

* Corresponding author. Tel.: +1 505 272 7626.
E-mail address: jemille@sandia.gov (J.E. Miller).

0926-3373/$ – see front matter. Published by Elsevier B.V.
doi:10.1016/j.apcatb.2007.09.010

component (BaO) to form the sulfate ($BaSO_4$). The sulfates are more stable than the nitrates and do not readily decompose during regeneration. Thus, the use of sulfur-containing fuels results in a continuous decline in NO_x storage capacity of NSR systems. A number of studies have focused on improving the tolerance of NSR catalysts to SO_2; however, no ultimate solution has been identified [3,4]. For example, it has been shown that addition of Rh inhibits sulfate formation, whereas Pt favors it [5]. Unfortunately, Rh was also shown to decrease the NO_x storage capacity [6]. The utilization of TiO_2 as a storage material in a Pt-Rh containing catalyst increased sulfur tolerance but similarly decreased NO_x storage capacity [7]. Yamakazi et al. [3] found that 10 wt.% Fe added to Pt–BaO/Al_2O_3 improved the catalyst's sulfur tolerance by inhibiting the growth of sulfate particles under oxidizing conditions and subsequently increasing the desorption of the sulfates under reducing conditions; no data on the impact of Fe addition on the NO_x storage capacity of the catalyst were given. Finally, it was reported [8] that addition of Cu to Pt/hydrotalcite, the hydrotalcite being the storage material, decreased the impact of SO_2 on the catalyst. In the present study, the effect of adding Cu to the benchmark catalyst, Pt–BaO/γ-Al_2O_3, has been investigated and a mechanism for the observed changes has been proposed.

2. Experimental

Four primary catalyst formulations, Pt–BaO/γ-Al_2O_3, Cu–BaO/γ-Al_2O_3, BaO/γ-Al_2O_3, and Pt–Cu–BaO/γ-Al_2O_3, were prepared and tested for NO_x storage reduction. Pt and Cu were supported on γ-Al_2O_3 by incipient wetness impregnation from $(NH_3)_2Pt(NO_2)_2$ and $Cu(NO_3)_2{\cdot}3H_2O$ precursors. In the case of Pt–Cu–BaO/γ-Al_2O_3, Cu was added prior to Pt. In each case, Ba was added last by incipient wetness impregnation of a barium acetate solution. After each impregnation step, the samples were calcined at 500 °C for 4 h. The target loadings were 1 wt.% Pt, 2 wt.% Cu, and 20 wt.% BaO. After the final calcination, the catalysts were ground and sieved to obtain a 60–100 mesh fraction. Samples of 2% Pt–20% BaO/γ-Al_2O_3 and 4% Cu–20% BaO/γ-Al_2O_3 were also prepared. Equal amounts of these samples were then physically mixed so that the combined sample had an overall metal content of 1 wt.% Pt, 2 wt.% Cu, and 20 wt.% BaO.

The NSR reaction was carried out at 380 °C and atmospheric pressure in a tubular fixed bed flow reactor loaded with ca. 0.25 g of catalyst. Both oxidizing (storage) and reduction (regenerating) conditions were simulated with the reactants consisting of NO, hydrocarbons ($C_3H_6/C_3H_8 = 3$), and O_2 in a balance of N_2 (Table 1). For the reduction condition, the gas mix was slightly oxidizing in the stoichiometric sense, although effectively reducing. The use of a highly reducing gas mix was avoided in order to challenge the catalyst and therefore help to highlight differences and changes in the materials. SO_2 was added to reducing and oxidizing gas mixtures as indicated in the text below. An automatic 4-port valve was used to switch between the two continuously flowing (volumetric space velocity 40,000 h^{-1}) mixtures so that the disturbance to the reactor was minimized. The reactor effluent was continuously analyzed for NO, NO_2, and N_2O by FTIR (Midac, 0.5 cm^{-1} resolution). The storage capacity, i.e. the amount of NO_x adsorbed, is measured during the storage cycle and is defined as the difference between the amount of nitrogen oxide fed to the reactor ($NO_{(inlet)}$) and the amount of nitrogen oxides leaving the reactor ($NO_{x(outlet)} = NO + NO_2 + 2N_2O$) integrated over a time period long enough for the storage media to be saturated. That is

$$\text{storage capacity}\ (\mu\text{mol/gcat}) = \frac{1}{\text{Cat.mass}}\left[\int_0^t \text{NO}_{(\text{inlet})}\,\text{d}t - \int_0^t \text{NO}_{x(\text{outlet})}\,\text{d}t\right]$$

The media is assumed to be saturated when $NO_{(inlet)} = NO_{x(outlet)}$. The NO_x conversion is determined during the reduction cycle and only accounts for the conversion of the NO being instantaneously fed to the reactor at that time. That is

$$\text{conversion}\ (\%) = 100 \times \frac{(\text{NO}_{(\text{inlet})} - \text{NO}_{x(\text{oulet})})}{\text{NO}_{(\text{inlet})}}$$

The amount of non-adsorbed NO_2 has been calculated at times to evaluate the oxidation activity of a given catalyst. That is

$$\text{Amount of non-adsorbed NO}_2\ (\mu\text{mol/gcat}) = \frac{1}{\text{Cat.mass}}\int_0^t \text{NO}_2\,\text{d}t$$

The catalysts were conditioned for 2 h under reaction conditions alternating between storage and reduction cycles prior to collecting the data presented here.

Temperature-programmed reduction (TPR) analyses were carried out on 0.5 g samples using a Micromeritics AutoChem 2910 apparatus equipped with a thermal conductivity detector (TCD). The samples were ramped from room temperature to ca. 950 °C at 10 °C/min in a 50 sccm flow of 10% H_2/Ar. In some cases, the samples were subjected to an in situ pretreatment prior to TPR analysis (see Section 3.5). Hydrogen chemisorption was carried out at ca. 50 °C using the same apparatus in pulse mode. Prior to the analyses, the samples were first reduced with 10% H_2/Ar at 280 °C for 7 h and then degassed in flowing Ar at 300 °C for 100 min.

Table 1
Compositions of the gas feeds during storage and reduction cycles

Cycle	NO (ppm)	O_2 (vol.%)	Propene and propane (vol.%)
Storage (for 30 min)	420	8	0.1
Reduction (for 10 min)	420	0.5	0.1

3. Results and discussion

3.1. Baseline NSR behavior

The concentration histories of NO, NO_2, N_2O and $NO_{x(oulet)}$ ($NO + NO_2 + 2N_2O$) in the effluent of a typical run over

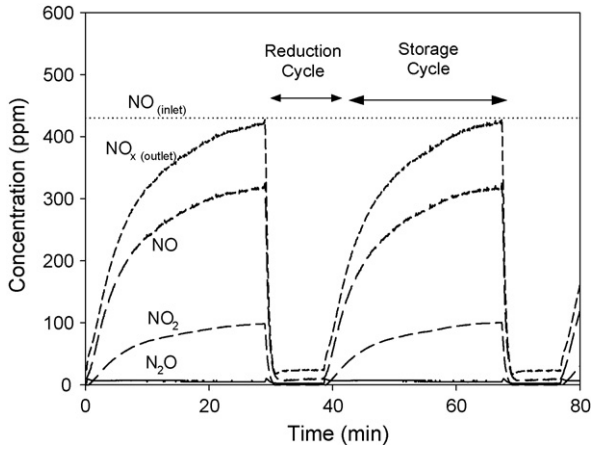

Fig. 1. Concentrations of N-containing species in effluent as a function of time during alternate storage and reduction cycling over Pt–BaO/γ-Al_2O_3 at 380 °C. Feed compositions are given in Table 1.

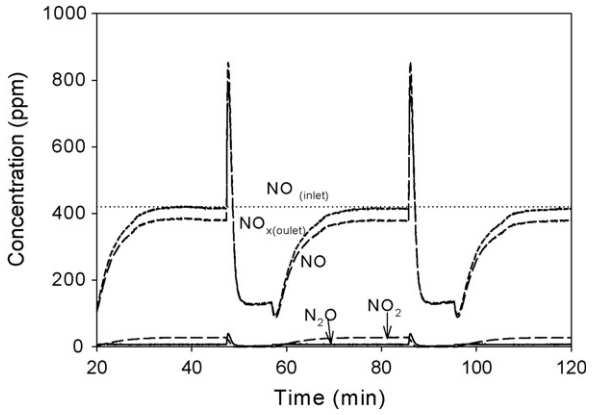

Fig. 2. Concentrations of N-containing species in effluent as a function of time during alternate storage and reduction cycling over Pt–Cu–BaO/γ-Al_2O_3 at 380 °C. Feed compositions are given in Table 1.

Table 2
Comparison of the performance of Pt–BaO/γ-Al_2O_3 and Pt–Cu–BaO/γ-Al_2O_3 during NSR reaction

Catalysts	Amount of NO_x adsorbed (μmol/gcat)	Conversion (%)	Amount of non-adsorbed NO_2 (μmol/gcat)
Pt–BaO/γ-Al_2O_3	108	91	74
Pt–Cu–BaO/γ-Al_2O_3	69	63	23

Pt–BaO/γ-Al_2O_3 at 380 °C are shown in Fig. 1. The inlet NO concentration is also shown for comparison. A similar NSR profile for Pt–Cu–BaO/γ-Al_2O_3 is shown in Fig. 2. The corresponding storage capacities, seen in Figs. 1 and 2 as the difference between the areas under the $NO_{(inlet)}$ and the $NO_{x(oulet)}$ curves during the storage cycles, and NO_x conversions are given in Table 2. Clearly, in the as-prepared form, Pt–BaO/γ-Al_2O_3 outperforms Pt–Cu–BaO/γ-Al_2O_3 in terms of NO_x storage capacity. Furthermore, there is greater conversion of NO to NO_2 during the storage cycle over the Pt–BaO/γ-Al_2O_3 formulation (Table 2). The as-prepared Pt–BaO/γ-Al_2O_3 also outperforms Pt–Cu–BaO/γ-Al_2O_3 in terms of reduction-cycle NO_x conversion. Although the reduction cycle is not highly reducing, NO_x conversion over the baseline Pt–BaO/γ-Al_2O_3 formulation is greater than 90%. The NO_x conversion is only 63% over the Cu-modified material under these challenging conditions. As expected under these conditions, only trace amounts of NH_3 (<5 ppm) were ever detected over either material. Neither catalyst produces a significant amount of N_2O.

One very notable difference between the materials is that a NO_x-breakthrough occurs in the case of the Cu-modified catalyst when switching the reaction from storage to reduction cycle (Fig. 2) that is not evident for the baseline material. NO_x breakthrough has been reported in other work, for example over Pt–BaO/γ-Al_2O_3 [9], over Pt–Rh–BaO/γ-Al_2O_3 [10,11] and over Pt–CaO/γ-Al_2O_3 [12]. Bogner et al. [10] suggested that NO_x breakthrough may result from sluggish reduction of the noble metal, the reduced metal being necessary for NO_x reduction. Fridell et al. [11] argued that the reduction of the noble metals is not a limiting step, but rather that the breakthrough could result from sweeping of NO_x by the hydrocarbons, or possibly by a combination of a transformation of the surface when switching from storage to reduction cycle and a high desorption rate of NO at the temperatures studied. In our case, the breakthrough has only been observed in catalysts containing Cu, that is Pt–Cu–BaO/γ-Al_2O_3 and Cu–BaO/γ-Al_2O_3 (NSR profile not shown). The conversion of NO to N_2 during the reduction cycle on these two catalysts is also relatively low. The NO_x breakthrough and the low reduction of NO are caused either by non-selective or slow reduction kinetics, by decreased affinity of the metal (Pt–Cu) to absorb NO_x, or a combination of several or all of these.

The effect of sulfur on the two materials was evaluated by introducing SO_2 to the cycling reaction stream either for 4 h at 90 ppm or for 12 h at 40 ppm. The results for the sulfur-exposed catalysts are provided in Table 3. As expected, the results show that both SO_2 protocols deactivated each of the catalysts to some degree. However, the lower concentration of SO_2 deactivated both catalysts to a lesser extent, even though the total SO_2 exposure was greater (480 ppm h versus 360 ppm h).

Table 3
Impact of SO_2 on the performances of Pt–BaO/γ-Al_2O_3 and Pt–Cu–BaO/γ-Al_2O_3

Catalyst	Amount of NO_x adsorbed (μmol/gcat)			Conversion (%)		
	Standard reaction	40 ppm SO_2-12 h	90 ppm SO_2-4 h	Standard reaction	40 ppm SO_2-12 h	90 ppm SO_2-4 h
Pt–BaO/γ-Al_2O_3	108	54	45	91	40	40
Pt–Cu–BaO/γ-Al_2O_3	69	56	53	63	35	30

That is, the impact of SO_2 on the catalysts is a function of concentration. More importantly, SO_2 had a more negative impact on the benchmark catalyst than on the Cu-modified catalyst, independent of SO_2 concentration. For example, the decrease in the storage capacity of Pt–BaO/γ-Al_2O_3 and Pt–Cu–BaO/γ-Al_2O_3 was 50% and 19%, respectively, for the 40 ppm-12 h case and 58% and 23%, respectively, for the 90 ppm-4 h case. Similarly, the decrease in the conversion is 56% compared to 44% for 40 ppm-12 h case and 56% compared to 52% for the 90 ppm-4 h case. Thus, even though Pt–BaO/γ-Al_2O_3 has a better initial performance than Pt–Cu–BaO/γ-Al_2O_3, after sulfur exposure the Cu-modified catalyst maintains a greater storage capacity. The impact on conversion is not as pronounced, but nonetheless Cu appears to have small a positive effect.

3.2. Cu loading

The impact of different Cu loading levels in Pt–Cu–BaO/γ-Al_2O_3 has been investigated, and the results for the NO_x storage capacity are shown in Fig. 3. In the absence of SO_2, the storage capacity decreases with increasing amounts of Cu. However, after exposure to SO_2 (90 ppm-4 h), the positive impact of Cu is apparent. Among the samples tested, a 2% loading of Cu resulted in the highest tolerance to SO_2.

3.3. Method of Cu addition

NSR was conducted on the 2% Cu–BaO/γ-Al_2O_3 and the commingled 2% Pt–20% BaO/γ-Al_2O_3 and 4% Cu–20% BaO/γ-Al_2O_3 sample both before and after SO_2 exposure (90 ppm-4 h). The results for these materials are compared to the results on Pt–BaO/γ-Al_2O_3 and Pt–Cu–BaO/γ-Al_2O_3 in Fig. 4. As expected, prior to SO_2 exposure Pt–BaO/γ-Al_2O_3 exhibited the highest storage capacity and conversion. The commingled material was initially very similar to the Pt–BaO/γ-Al_2O_3 sample with high conversion and only a slightly reduced storage capacity. In contrast, the Cu–BaO/γ-Al_2O_3 was similar to Pt–Cu–BaO/γ-Al_2O_3 in terms of storage capacity but had very little activity for NO_x reduction. These results confirm the necessity of the noble metal for NO_x reduction and suggest that Cu–BaO/γ-Al_2O_3 and Pt–Cu–BaO/γ-Al_2O_3 have similar capacity to oxidize NO.

After SO_2 exposure, Pt–Cu–BaO/γ-Al_2O_3 maintained the highest storage capacity. That is, commingled Pt and Cu and Cu alone both have a lesser degree of sulfur tolerance than Pt–Cu–BaO/γ-Al_2O_3. These results indicate that Pt and Cu must be in close proximity to one another to confer sulfur tolerance upon the storage component of the catalyst. From a NO_x conversion standpoint the benefit of Cu is less clear. All the samples showed a significant loss of ca. 45–50% of the initial NO_x conversion independent of the presence of Cu or the method of its addition.

Taken as a whole, the results suggest that when in close proximity, Cu alters the Pt such that the activity for the oxidation of SO_2 is significantly decreased, while the capacity to oxidize NO is altered to a lesser degree. It is unclear why Pt–Cu favors the oxidation of NO to NO_2 over SO_2 to SO_3. However, it has been suggested that NO_2, formed by oxidation of NO, might participate in the oxidation of SO_2 to SO_3, if it is not rapidly converted to nitrate [8]. This proposition was based on the observation that Pt/hydrotalcite (HT) treated with SO_2 in the presence of air alone deactivates less than when SO_2 is

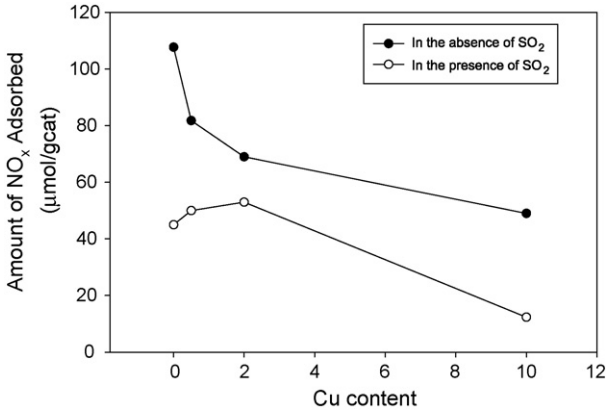

Fig. 3. Impact of Cu loading and SO_2 exposure (90 ppm for 4 h) on NO_x storage capacity of modified Pt–BaO/γ-Al_2O_3. Pt loading is 1 wt.% for all samples in figure.

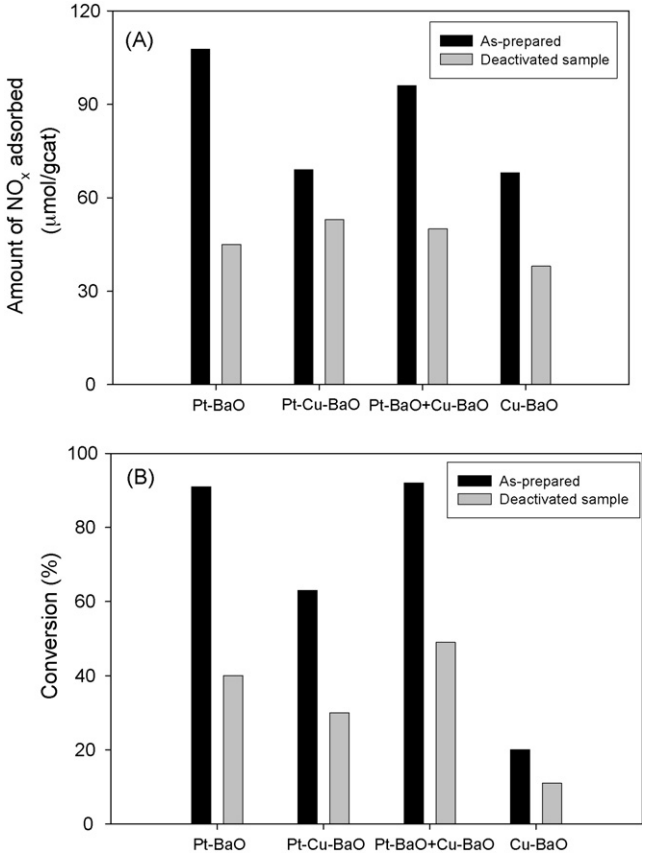

Fig. 4. (A) Amount of NO_x adsorbed on and (B) conversion of NO_x over Pt–BaO/γ-Al_2O_3, Pt–Cu–BaO/γ-Al_2O_3, (Pt–BaO/γ-Al_2O_3 + Cu–BaO/γ-Al_2O_3), and Cu–BaO/γ-Al_2O_3.

Table 4
Effect of H_2 pretreatment on Pt–BaO/γ-Al_2O_3 and Pt–Cu–BaO/γ-Al_2O_3

Reduction (reaction conditions)	Amount of NO_x adsorbed (μmol/gcat)			NO_x conversion (%)		
	Pt–BaO/γ-Al_2O_3	Pt–Cu–BaO/γ-Al_2O_3	Cu–BaO/γ-Al_2O_3	Pt–BaO/γ-Al_2O_3	Pt–Cu–BaO/γ-Al_2O_3	Cu–BaO/γ-Al_2O_3
None (standard conditions)	108	69	68	91	63	20
None (SO_2; 90 ppm-4 h)	45	53	38	40	30	11
H_2 (standard conditions)	116	62	–	92	45	–
H_2 (SO_2; 90 ppm-4 h)	61	39	–	38	29	–
Reduction cycle (standard conditions)	104	67	–	92	66	–
Reduction cycle (SO_2; 90 ppm-4 h)	43	55	–	38	29	–

added during NSR. Therefore, there may be a direct link between the rate of NO_2 formation and the oxidation of SO_2.

3.4. Effect of catalyst reduction on performance

The impact of reducing the Pt–BaO/γ-Al_2O_3 and Pt–Cu–BaO/γ-Al_2O_3 with H_2 for 2 h at 380 °C was investigated as well as the impact of 2 h reduction with the reduction cycle gas mixture. The results for NSR over the reduced materials, both in the absence and in the presence of SO_2, are presented in Table 4. For Pt–BaO/γ-Al_2O_3, the H_2 reduction step had an overall positive impact on the catalyst. The storage capacity was increased slightly from 108 to 116 μmol/gcat, and the negative impact of SO_2 on the storage capacity was diminished. The loss in storage capacity was decreased from 58% for the as-prepared catalyst to 47% for the H_2-pretreated catalyst. The impact of H_2 reduction on the NO_x conversion was minimal. These results are consistent with previous reports that fully reduced Pt is more active for the oxidation of NO_x [13].

In contrast to the Pt–BaO/γ-Al_2O_3, the H_2 reduction of Pt–Cu–BaO/γ-Al_2O_3 had a negative impact on NSR performance. The storage capacities with and without sulfur exposure were both diminished. The loss in the storage capacity upon sulfur exposure increased from 23% for the as-prepared material to 37% for the H_2-reduced material. Moreover, H_2 reduction of Pt–Cu–BaO/γ-Al_2O_3 decreased the NO_x conversion, although after sulfur exposure the NO_x conversions for both samples were similar. Comparing these results to the performance of Cu–BaO/γ-Al_2O_3 suggests that the H_2 reduction has produced a material wherein the catalytic properties are dominated by the Cu component. For example, the reduced Pt–Cu–BaO/γ-Al_2O_3 has storage capacities of 62 and 39 μmol/gcat before and after sulfur exposure, while the Cu–BaO/γ-Al_2O_3 has storage capacities of 68 and 38 μmol/gcat under similar conditions. Furthermore, the Pt-catalyzed NO_x conversion over the reduced Pt–Cu–BaO/γ-Al_2O_3 exceeds only that of Cu–BaO/γ-Al_2O_3.

In contrast to reduction with hydrogen, the pretreatment of the samples under the reduction cycle conditions did not have any impact on their performance. This is an indication that the typical reaction conditions are unlikely to result in a catalyst reduction that alters catalytic behavior. However, the potential for transformation with extended time-on-stream or if a more highly reducing reductive-cycle environment is provided cannot be ruled out.

3.5. TPR- and H_2-chemisorption analyses

The results of TPR analysis are shown in Fig. 5. The TPR profile of BaO/γ-Al_2O_3 (curve a) is characterized by a large peak centered at ca. 915 °C with a shoulder at ca. 780 °C. A small broad peak at ca. 550 °C can be seen as well. All peaks correspond to the reduction of barium compounds with the high temperature peak being the reduction of barium carbonate. The reduction profile of Pt–BaO/γ-Al_2O_3 (curve b) shows two primary peaks. The high temperature features (large peak at ca. 850 °C with a shoulder at ca. 775 °C) are attributed to the reduction of $BaCO_3$. The second large peak, centered at ca. 460 °C, may be attributed to the reduction of Pt. The TPR profile of Cu–BaO/γ-Al_2O_3 (curve c) exhibits two low temperature peaks, ca. 226 °C and ca. 336 °C, attributable to CuO [14,15] and Cu_2O [15], respectively. As before, the high temperature features are attributable to carbonates. The commingled sample (Pt–BaO/γ-Al_2O_3 + Cu–BaO/γ-Al_2O_3) (curve d) shows a profile similar to a superposition of the individual profiles of Pt–BaO/γ-Al_2O_3 (curve b) and of Cu–BaO/γ-Al_2O_3 (curve c). On the other hand, the profile of Pt–Cu–BaO/γ-Al_2O_3 (curve e) presents a broad peak with a maximum at ca. 237 °C and a shoulder at ca. 178 °C and a peak corresponding to the reduction of barium carbonates at ca. 915 °C. The individual reduction peaks of Pt and Cu are not seen, indicative of a Pt/Cu interaction not present in the commingled sample.

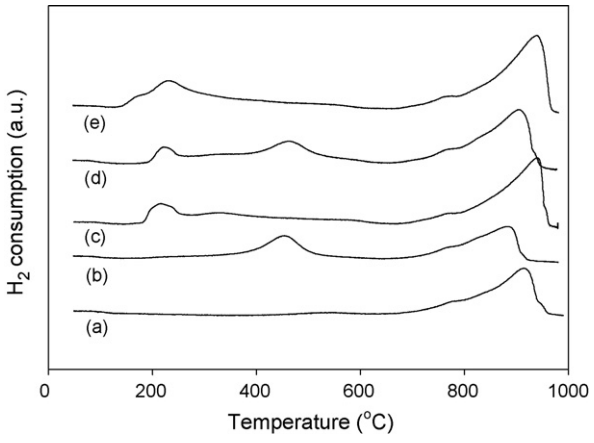

Fig. 5. TPR profiles of (a) BaO/γ-Al_2O_3, (b) Pt–BaO/γ-Al_2O_3, (c) Cu–BaO/γ-Al_2O_3, (d) Pt–BaO/γ-Al_2O_3 + Cu–BaO/γ-Al_2O_3, and (e) Pt–Cu–BaO/γ-Al_2O_3.

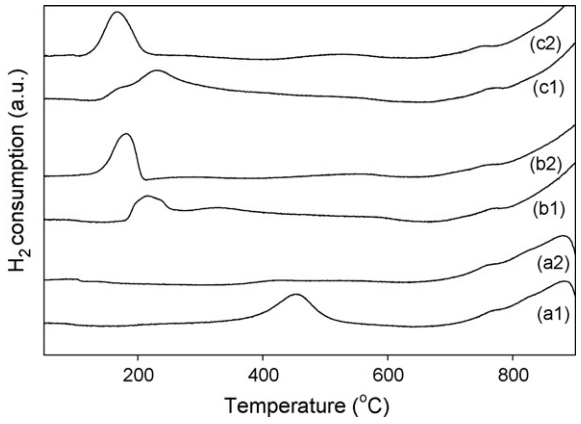

Fig. 6. Impact of H_2 reduction on the TPR profiles of (a1 and a2) Pt–BaO/γ-Al_2O_3, (b1 and b2) Cu–BaO/γ-Al_2O_3, and (c1 and c2) Pt–Cu–BaO/γ-Al_2O_3: (1) as-prepared, (2) reduced and re-oxidized.

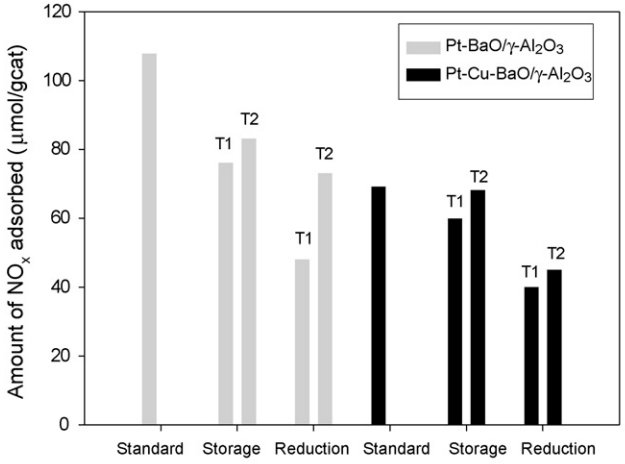

Fig. 7. Amount of NO_x adsorbed on Pt–BaO/γ-Al_2O_3 and on Pt–Cu–BaO/γ-Al_2O_3 after deactivation with SO_2 under storage or reduction cycle. T1: first cycle after ending SO_2; T2: cycle beginning 200 min after ending SO_2.

Similar TPR analysis was carried out on samples of Pt–BaO/γ-Al_2O_3, Cu–BaO/γ-Al_2O_3, and Pt–Cu–BaO/γ-Al_2O_3 that had first been reduced with H_2 at 380 °C for 4 h and then re-oxidized at 350 °C for 12 h in situ prior to carrying out the analysis. The results are summarized and compared to their as-prepared counterparts in Fig. 6. In the case of Pt–BaO/γ-Al_2O_3 (curves a1 and a2), it is clear that the Pt was reduced and remained in the reduced state during the subsequent exposure to oxygen. The Cu–BaO/γ-Al_2O_3 was also altered by the pretreatment, with a single low-temperature reduction feature (curve b2) replacing the two features previously associated with oxides of Cu (curve b1). Surprisingly, the TPR profile of the pretreated Pt–Cu–BaO/γ-Al_2O_3 (c2) is almost identical to that of the pretreated Cu–BaO/γ-Al_2O_3 sample (b2). That is, there is no longer any evidence in the TPR profile of an interaction between Cu and Pt. These results are consistent with the results of the NSR reaction over H_2-reduced catalysts.

H_2 chemisorption was carried out on Pt–BaO/γ-Al_2O_3 and Pt–Cu BaO/γ-Al_2O_3 to probe the Pt dispersion independent of the Cu [16,17]. Cu addition to the benchmark catalyst significantly decreases the dispersion of Pt from 48% for Pt–BaO/γ-Al_2O_3 to 8%, Pt–Cu–BaO/γ-Al_2O_3. Note that this result is only indicative of the state of the sample after H_2 reduction. Due to the presence of Pt (and possibly other) oxides, reliable chemisorption data cannot be obtained for the as-prepared samples.

3.6. Sulfur exposure during storage or reduction cycle only

The impact of SO_2 addition during only the storage or the reduction cycle was investigated. Pt–BaO/γ-Al_2O_3 and Pt–Cu–BaO/γ-Al_2O_3 were pretreated under reduction or storage cycle conditions in the presence of 90 ppm SO_2 for 2 h, after which the flow of SO_2 was stopped, but the experiment continued. Fig. 7 compares the storage capacities of the as-prepared materials to the treated samples at two points: T1, the first cycle recorded after the SO_2 flow was suspended, and T2, the cycle beginning 200 min after the SO_2 flow was ended. It is clear from the figure that in both cases the addition of SO_2 during the reduction cycle has greater negative impact than addition during the storage cycle. This is especially true for the Pt–Cu–BaO/γ-Al_2O_3 sample, for which only a slight decrease in storage capacity resulted from the storage cycle exposure. It is also clear that each catalyst has at least some capacity to recover once sulfur is removed from the feed stream. However, the recovery is most pronounced for the Pt–BaO/γ-Al_2O_3 samples exposed to sulfur under reducing conditions, particularly when compared to the similarly treated Cu-modified sample which showed only a very modest recovery. Note also that the storage capacity of the Pt–Cu–BaO/γ-Al_2O_3 sample treated with SO_2 during the storage cycle was almost fully recovered with time-on-stream.

3.7. Discussion

The addition of Cu to Pt–BaO/γ-Al_2O_3 yields an NSR material that is more tolerant to the presence of SO_2 in the exhaust gas. More specifically, the addition of Cu greatly minimizes the loss of storage capacity resulting from sulfur poisoning of the BaO. Only a small improvement in NO_x conversion is realized. These benefits are realized at the expense of an initial loss of storage capacity. Given that Cu–BaO/γ-Al_2O_3 is a poor catalyst and not especially sulfur tolerant, perhaps the simplest plausible explanation for the beneficial effect of Cu is that it is not a genuine modifier of the catalytic chemistry, but rather a sulfur getter that competes with BaO to capture SO_2 as $CuSO_4$, thus leaving barium sites available to form nitrate [18]. If this were the case, one would expect that increasing the Cu content would increase the sulfur capacity as has been demonstrated for Cu-based sorbers for flue gas applications [19], and that the sulfur tolerance would also thus be improved. In the present case, however, the 10% Cu-modified sample has less sulfur tolerance than the 2% Cu sample, strongly suggesting a different mechanism is at work. Furthermore, a comparison of the NSR results for Pt–Cu–BaO/γ-Al_2O_3 and the similar commingled sample shows that Cu

must be in close proximity to the Pt in order to confer the benefit of improved sulfur tolerance. Again, this would not be expected if Cu were acting only as a sulfur trap, particularly in the light of the fact that SO_3 formed over Pt is known to be capable of migrating over an alumina support and even between particles [20]. Finally, $CuSO_4$ is significantly less stable than $BaSO_4$ and thus Cu should provide little benefit as a sulfur getter as $BaSO_4$ should form preferentially in the presence of SO_3. Kinetic limitations could of course shift the outcome away from the thermodynamic equilibrium state. However, in several instances researchers have found no evidence of $CuSO_4$ in aged Cu/CaO [21] or Cu/BaO-based [22,23] sulfur traps, although the data does not allow its presence to be conclusively ruled out. To summarize, the evidence strongly suggests that copper plays a more complex role than that of a simple trap.

Looking further, the TPR results suggest that a new Pt/Cu bimetallic phase is formed when the two metals are impregnated on the same support. The presence of a bimetallic phase containing both Pt and Cu was confirmed by transmission electron microscopy coupled with energy-dispersive X-ray spectroscopy (Fig. 8). Given the requirement of close proximity, it is likely that the bimetallic phase is responsible for the catalyst improvements. That is, the incorporation of Cu in the Pt catalyst produces a mixed Pt/Cu surface that confers sulfur tolerance. This model is consistent with the observation that there is an optimum Cu loading. When the Cu content is too large (as for the 10% Cu sample), the surface of the bimetallic particles and hence the catalyst behavior is dominated by the inferior catalyst, Cu.

This simple picture of the catalyst surface is somewhat complicated by the TPR results for the H_2-reduced samples. First, consider that the H_2-reduced Pt–BaO/γ-Al_2O_3 shows no Pt peaks after reduction and re-oxidation. This could result from an encapsulation of Pt by BaO during reduction of Pt–BaO/γ-Al_2O_3 as has been suggested by Fanson et al. [24]. However, the NSR and chemisorption results for the reduced Pt–BaO/γ-Al_2O_3 indicate that Pt remains accessible. Therefore, these results are more consistent with the formation of Pt metal particles that are stable towards re-oxidation than an encapsulation scenario.

Now consider the results for the reduced Pt–Cu–BaO/γ-Al_2O_3 catalyst. After reduction and re-oxidation, the TPR profile no longer shows evidence of a bimetallic phase, but rather, it greatly resembles that of the reduced Cu–BaO/γ-Al_2O_3 sample. Recalling that reduced Pt–BaO/γ-Al_2O_3 has no TPR features associated with Pt, this is consistent with a decomposition of the bimetallic phase into distinct Pt and Cu phases. However, it is also consistent with a model in which the surface of the Pt/Cu phase becomes enriched in Cu upon reduction, i.e. an encapsulation of Pt by Cu. The NSR results favor this second possibility. If the catalyst had phase separated, the NSR performance would be expected to be similar to that of the commingled sample (Fig. 4). Instead, it more closely resembles that of Cu–BaO/γ-Al_2O_3. Furthermore, the encapsulation scenario is consistent with the very low dispersion of Pt in the Pt–Cu–BaO/γ-Al_2O_3 material after reduction.

It has been previously reported that surfaces of Pt–Cu/γ-Al_2O_3 are enriched in Cu relative to the bulk composition [25].

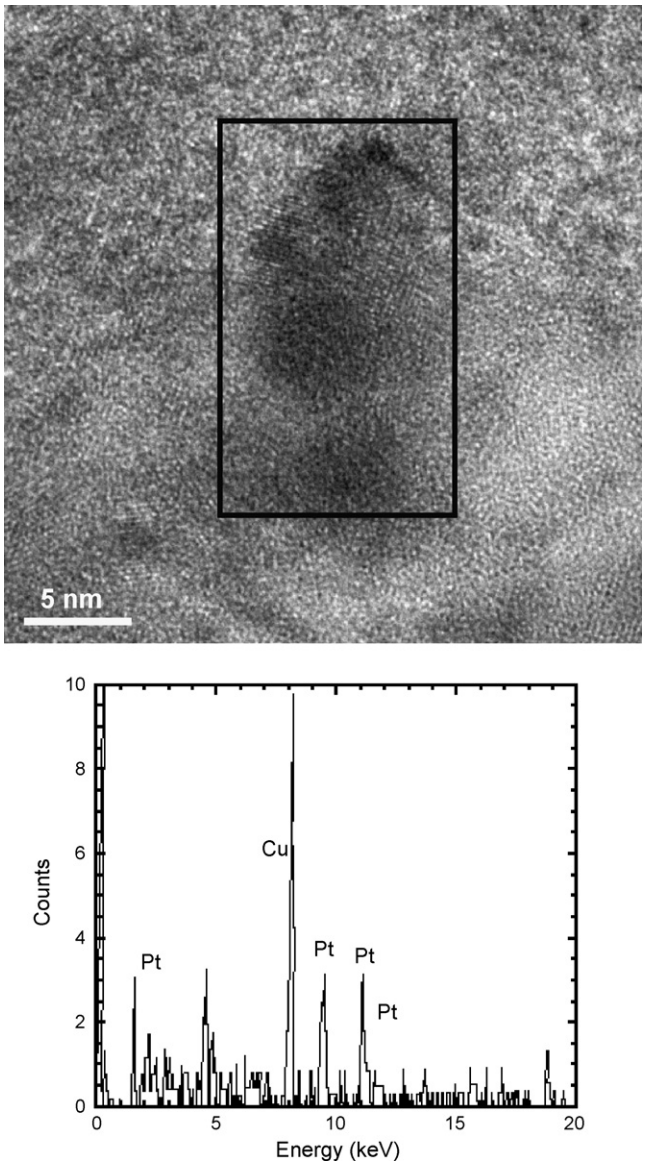

Fig. 8. TEM micrograph of Pt–Cu–BaO/γ-Al_2O_3. Accompanying EDS spectra shows the highlighted particle contains both Pt and Cu. A carbon-coated nylon grid was utilized to avoid a contribution to the Cu EDS signal originating from the TEM grid.

Thus, it is possible that in all instances the surface of the bimetallic phase in Pt–Cu–BaO/γ-Al_2O_3 is relatively Cu-rich. However, the reduction of the catalyst with H_2 clearly accentuates this phenomenon. The pretreatment of the catalyst under milder reducing conditions (the conditions of the reduction cycle) does not produce the same result. Still, such a transformation cannot be ruled out for a much longer exposure time or more highly reducing reaction conditions.

Insight into the role of Cu is provided by the studies wherein SO_2 exposure was limited to only the storage or reduction cycles. First, consider the baseline Pt–BaO/γ-Al_2O_3 formulation with storage cycle exposure to SO_2. Previous studies have clearly shown that the loss in storage capacity of these materials results from the oxidation of SO_2 to SO_3 followed by the reaction of SO_3 with BaO to form sulfates. The requirement that

Table 5
Impact of storage or reduction cycle deactivation on the amount of NO_2 produced over Pt–BaO/γ-Al_2O_3 and Pt–Cu–BaO/γ-Al_2O_3 (the NO_x totals are given in μmol/gcat)

Pretreatment		Pt–BaO/γ-Al_2O_3			Pt–Cu–BaO/γ-Al_2O_3		
		NO_x adsorbed	Non-adsorbed NO_2	Total amount of NO_2	NO_x adsorbed	Non-adsorbed NO_2	Total amount of NO_2
None		108	74	182	69	23	92
SO_2 storage	T1[a]	76	70	146	59	37	96
	T2	80	90	170	68	26	94
SO_2 reduction	T1	48	63	111	40	7	47
	T2	75	94	169	45	7	52

[a] T1: first cycle after ending SO_2; T2: cycle beginning 200 min after ending SO_2.

SO_2 be oxidized should effectively restrict this mechanism to the storage cycle. As expected from the stability of $BaSO_4$, there is little improvement in storage capacity with TOS after sulfur exposure is terminated (Fig. 7). Now consider that very little loss in storage capacity occurs for Pt–Cu–BaO/γ-Al_2O_3 during the storage cycle. This suggests that the bimetallic phase in this catalyst does not effectively oxidize SO_2 to SO_3 and that sulfur therefore passes out of the system in the effluent gas. That is, the Cu in the bimetallic phase moderates the propensity of the Pt to oxidize SO_2. Of course, the oxidation of NO to NO_2 is also impacted. The total amount of NO_2 produced over this catalyst is approximately half of that produced over Pt–BaO/γ-Al_2O_3 (Table 5), and this may contribute to the loss in initial storage capacity. The more significant effect however appears to be on SO_2, although SO_2 conversion was not directly measured.

Interestingly, there is no effect of storage-cycle SO_2 on the total amount of NO_2 produced over Pt–Cu–BaO/γ-Al_2O_3 (Table 5). The fact that the total amount of NO_2 is the same before and after sulfur exposure indicates that the sulfur has no effect on the Pt during the storage cycle. In contrast, the total amount of NO_2 produced over Pt–BaO/γ-Al_2O_3 is reduced by storage-cycle SO_2, although it recovers with TOS after exposure (Table 5). This suggests that diminished activity of the bimetallic phase for SO_2 oxidation may be associated with a reduced affinity for SO_2 adsorption relative to Pt.

Very different results are obtained when SO_2 exposure is limited to the reduction cycles. First, in agreement with the literature [26], we observed that Pt–BaO/γ-Al_2O_3 suffers a greater loss in storage capacity when exposed to SO_2 during reduction cycles than when exposed during storage cycles. It has been postulated that barium sites in the vicinity of Pt are selectively poisoned during the reduction cycle, whereas bulk barium sites are poisoned during the storage cycle [26]. In our case, there was a significant, but not complete, recovery with TOS after SO_2 was removed from the gas feed. This recovery suggests that it was Pt rather than BaO that was initially poisoned during the reduction cycle. This interpretation is bolstered by the fact that in this case both the storage capacity and the oxidation of NO to NO_2 were affected by the SO_2 (Table 5). The fact that the storage capacity was not fully recovered may be attributable to the oxidation of SO_2 or other sulfur species adsorbed on Pt to SO_3 and subsequent $BaSO_4$ formation upon switching to the storage cycle. The almost complete recovery of the activity for NO oxidation to NO_2 (Table 5) supports this scenario.

Similar to the results for Pt–BaO/γ-Al_2O_3, exposure of Pt–Cu–BaO/γ-Al_2O_3 to SO_2 during the reduction cycle resulted in a greater loss of storage capacity. However, in contrast to the results for Pt–BaO/γ-Al_2O_3, the capacity hardly recovered with TOS after SO_2 flow was stopped. In addition, as was the case with Pt–BaO/γ-Al_2O_3 material, the NO to NO_2 reaction over Pt–Cu–BaO/γ-Al_2O_3 was stifled by the addition of SO_2 during the reduction cycle. In this case however, the activity for NO oxidation did not recover. As before, the impact of SO_2 addition during the reduction cycle on NO oxidation suggests that the metals (Pt and Cu) were poisoned by SO_2 exposure during the reduction cycle. However, the lack of recovery suggests that the sulfur was not removed from the metal sites by subsequent oxidation. This is consistent with our previous assertion that the Cu-modified Pt does not readily oxidize SO_2 and it may indicate that recalcitrant sulfur compounds were formed with the Cu component of the bimetallic particles under reducing conditions.

4. Conclusions

The impact of Cu addition to Pt–BaO/γ-Al_2O_3 on the NSR reaction has been investigated in the presence and in the absence of SO_2. The addition of Cu to the catalyst decreases the initial NO_x storage capacity but improves the sulfur tolerance of the material. That is, SO_2 has a lesser impact on the remaining storage capacity, and thus after sulfur exposure the storage capacity of the Cu-modified material can exceed that of the baseline catalyst. The persistence of this effect after extended time-on-stream and after high temperature excursions or regeneration cycles remains to be determined. It has been established that the efficacy of Cu results from the formation of a bimetallic phase, Pt–Cu, that appears to moderate the catalyst's activity for SO_2 oxidation during the storage cycle. By limiting the formation of SO_3, the formation of capacity-consuming $BaSO_4$ is also limited. The moderation in SO_2 oxidation activity may result from a reduced affinity for SO_2 adsorption. The activity for NO oxidation is also somewhat reduced by Cu addition, but not eliminated.

The mechanism for deactivation during the reduction cycle differs from that during the storage cycle. Furthermore, the deactivation mechanism of the baseline material during the

reduction cycle differs from that of the Cu-modified material. The results are consistent with a model wherein sulfur blocks Pt sites on the baseline material during the reduction cycle. During subsequent storage cycles, the sulfur is oxidized and desorbs from the Pt and activity is restored. However, some of the resulting SO_3 reacts with the BaO to form $BaSO_4$, and there is a partial loss of storage capacity. Sulfur also blocks Pt and possibly Cu sites on Pt–Cu–BaO/γ-Al_2O_3 under reducing conditions. However, the sulfur is not removed by oxidation during the subsequent storage cycle, and hence activity is not restored. The formation of stable compounds of sulfur and Cu cannot be ruled out in this case.

Acknowledgements

This work has been funded by the Department of Energy Office of Transportation Technology. Sandia is a multiprogram laboratory operated by Sandia Corporation, a Lockheed Martin Company, for the United States Department of Energy's National Nuclear Security Administration under contract DE-AC04-94AL85000.

References

[1] S. Matsumoto, Y. Ikeda, H. Suzuki, M. Ogai, N. Miyoshi, Appl. Catal. B 25 (2000) 115.
[2] N. Miyoshi, S. Matsumoto, K. Katoh, T. Tanaka, J. Harada, N. Takahashi, K. Yokota, M. Suguira, K. Kasahara, SAE Technical paper 950809, 1995.
[3] K. Yamakazi, T. Suzuki, N. Takahashi, K. Yokota, M. Sugiura, Appl. Catal. B 30 (2001) 459.
[4] C.H. Sedlmair, K. Seshan, A. Jentys, J.A. Lercher, Res. Chem. Intermed. 29 (2003) 257.
[5] H. Mahzoul, L. Limoisy, J.F. Brilhac, P. Gilot, J. Anal. Appl. Pyrolysis 56 (2000) 179.
[6] H. Abdulhamid, E. Fridell, M. Skoglundh, Appl. Catal. B 62 (2006) 319.
[7] H.Y. Huang, R.Q. Long, R.T. Yang, Appl. Catal. B 33 (2001) 127.
[8] G. Centi, G. Fornasari, C. Gobbi, M. Livi, F. Trifiro, A. Vaccari, Catal. Today 73 (2002) 287.
[9] L. Olsson, E. Fridell, M. Skoglundh, B. Andersson, Catal. Today 73 (2002) 263.
[10] W. Bogner, M. Kramer, B. Krutzsch, S. Pischinger, D. Voigtlander, G. Wenninger, F. Wirbeleit, M.S. Brogan, R.J. Brisley, D.E. Webster, Appl. Catal. B 7 (1995) 153.
[11] E. Fridell, M. Skoglundh, B. Westerberg, S. Johansson, G. Smedler, J. Catal. 183 (1999) 196.
[12] H.Y. Huang, R.Q. Long, R.T. Yang, Energy Fuels 15 (2001) 205.
[13] L. Olsson, E. Fridell, J. Catal. 210 (2002) 340.
[14] G. Fierro, M. Lo Jacono, M. Inversi, P. Porta, R. Lavecchia, F. Cioci, J. Catal. 148 (1994) 709.
[15] P. Granger, J.M. Dumas, J. Barbier, J. Chim. Phys. 92 (1995) 1557.
[16] M.T.F. Mendes, M. Schmal, Appl. Catal. A 163 (1997) 153.
[17] C.G. Bond, N.S. Namijo, J. Catal. 118 (1989) 507.
[18] Q. Liu, Z. Liu, G. Xie, Z. Huang, Catal. Lett. 101 (2005) 27.
[19] K.S. Yoo, S.D. Kim, S.B. Park, Ind. Eng. Chem. 33 (1994) 1786.
[20] X. Wei, X. Liu, M. Deeba, Appl. Catal. B 58 (2005) 41.
[21] E. Schreier, R. Eckelt, M. Richter, R. Fricke, Appl. Catal. B 65 (2006) 249.
[22] H. Dathe, A. Jentys, P. Haider, E. Schreier, R. Fricke, J.A. Lercher, Phys. Chem. Chem. Phys. 8 (2006) 1601.
[23] H. Dathe, A. Jentys, J.A. Lercher, J. Phys. Chem. B 109 (2005) 21842.
[24] P.T. Fanson, M.R. Horton, W.N. Delgass, J. Lauterbach, Appl. Catal. B 46 (2003) 393.
[25] P.C. Liao, J.J. Carberry, T.H. Fleisch, E.E. Wolf, J. Catal. 74 (1982) 307.
[26] E. Fridell, H. Persson, L. Olsson, B. Westerberg, A. Amberntsson, M. Skoglundh, Topics Catal. 16/17 (2001) 133.